Journal of Catalysis **202,** 14–24 (2001)
doi:10.1006/jcat.2001.3249, available online at http://www.idealibrary.com on IDEAL®

Hydrogen Spillover from NiO to the Large Surface Area CeO_2–ZrO_2 Solid Solutions and Activity of the NiO/CeO_2–ZrO_2 Catalysts for Partial Oxidation of Methane

Tatsuya Takeguchi,[1] Shin-nosuke Furukawa, and Masashi Inoue

Department of Energy and Hydrocarbon Chemistry, Graduate School of Engineering, Kyoto University, Sakyo-ku, Kyoto 606-8501, Japan

Received August 1, 2000; revised April 12, 2001; accepted April 18, 2001

Reduction behaviors of NiO-modified large surface area CeO_2–ZrO_2 solid solutions were examined by the temperature-programmed reduction technique. NiO modification of the CeO_2–ZrO_2 solid solution lowered the reduction temperature of the solid solution. At the reduction stage of the CeO_2–ZrO_2 solid solution, NiO was the sole species observed by XRD. Therefore, NiO particles apparently facilitated the reduction of the solid solution, lowering its reduction temperature. The activity of the NiO/CeO_2–ZrO_2 catalysts for partial oxidation of methane to H_2 and CO increased with an increase of oxygen storage capacity of the CeO_2–ZrO_2 solid solutions. The NiO particles having strong interaction with the support showed high stability for partial oxidation of methane, while the NiO particles having weak interaction produced a large amount of coke (carbon nanotubes).

Key Words: **NiO/CeO_2–ZrO_2 catalyst; hydrogen spillover from NiO; large surface area CeO_2–ZrO_2; partial oxidation of methane; oxygen storage capacity; carbon nanotube.**

1. INTRODUCTION

Ceria is used as a promoter for many catalysts, such as three-way automobile catalysts, because the oxygen storage property of ceria plays the important role of enhancing catalytic activity under reducing and oxidizing conditions (1–3). Moreover, ceria improves the thermal stability of the alumina support, thereby stabilizing the catalyst metal particles (1–3).

On the other hand, much attention has been paid to the fuel cells because they hardly produce NO_X. For the fuel cells, it is desired to produce hydrogen more efficiently. Hydrogen is now produced by steam reforming of hydrocarbons, and in the future natural gas predominantly composed of methane will be used more widely as the raw hydrocarbon. Partial oxidation of methane is another candidate for the hydrogen process. Since steam reforming of methane is an endothermic reaction, a combination of reforming with combustion of methane to yield CO_2 and H_2O will reduce energy consumption by hydrogen production. Whereas steam reforming is operated in huge-scale plants, partial oxidation of methane to CO and H_2 can economically be carried out in smaller scale plants since the latter is an exothermic reaction. For partial oxidation of methane, operation conditions around the catalyst strongly depend on temperature, the position at which catalysts were packed, methane/O_2 ratio, and the catalytic activity (4). Therefore, the catalysts are required to work under various conditions, and improvement in stability of the catalysts is desired. A number of efforts have been devoted to increase the stability of Ni catalysts, and it was reported that catalytic activity and thermal stability were improved by using CeO_2 as the support (5, 6) or promoter (7, 8).

On the other hand, it is well known that CeO_2–ZrO_2 solid solutions also have oxygen storage properties. Graziani *et al.* investigated the redox properties of CeO_2–ZrO_2 solid solutions by the temperature-programmed reduction (TPR) technique (9–15) and reported that TPR of the Rh-loaded CeO_2–ZrO_2 solid solution with a low Ce content showed a peak at 823 K, corresponding to surface reduction of the solid solution, together with a broad signal at around 1073 K, while TPR of CeO_2 showed a peak at 1100 K (9), corresponding to reduction of bulk CeO_2 (3). Modification of CeO_2–ZrO_2 with noble metals such as Rh, Pt, and Pd considerably decreased the reduction temperature, and it was concluded that hydrogen atoms formed by dissociative adsorption on the noble metals were spilled over to CeO_2–ZrO_2 (11). Hydrogen spillover on ZrO_2 supports was also suggested for Pt/ZrO_2 (16, 17).

In this paper, CeO_2–ZrO_2 solid solutions having large surface areas (18, 19) are dealt with, and apparent hydrogen spillover phenomena (20) from NiO will be discussed. The performance of the Ni/CeO_2–ZrO_2 catalysts for the partial oxidation of methane to H_2 and CO is also reported.

[1] To whom correspondence should be addressed. Fax: (81)75-753-3352. E-mail: takeguch@scl.kyoto-u.ac.jp.

0021-9517/01 $35.00

2. EXPERIMENTAL

2.1. Catalyst Preparation

The CeO_2–ZrO_2 solid solutions and ZrO_2 having large surface areas were prepared by the glycothermal method (18, 19). Zirconium tetrapropoxide (25 g; Mitsuwa Pure Chemicals) and a desired amount of cerium acetate were mixed with 100 ml of 1,4-butanediol in a test tube, which was then set in a 300-ml autoclave. An additional 50 ml of 1,4-butanediol was added to the gap between the test tube and the autoclave wall. The gas phase in the autoclave was replaced with nitrogen. The mixture was heated from room temperature to 573 K at a rate of 2.3 K min^{-1} and kept at that temperature for 2 h. The resulting powders were washed with methanol, dried at room temperature for several days, and calcined at 673 K for 30 min. These samples were designated ZrO_2(GT) and $Ce_xZr_{1-x}O_2$(GT). A ZrO_2 sample, JRC-ZRO-1, supplied by the Catalysis Society of Japan was used as a reference, which was designated ZrO_2(R). For comparison, a CeO_2–ZrO_2 solid solution was also prepared by the co-precipitation method (21). In 100 ml of water, 1.211 g of $Ce(NO_3)_3 \cdot 2NH_4NO_3 \cdot 4H_2O$ and 5 g of $ZrO(NO_3)_2$ were dissolved, and to the solution was added a 10.79-g portion of $H_2C_2O_4 \cdot 2H_2O$ in 150 ml of water. The resulting gel was washed with water, dried at room temperature for several days, and calcined at 1073 K for 30 min. This sample was designated $Ce_{0.25}Zr_{0.75}O_2$(CP).

NiO loading was carried out by the impregnation method: 1 ml of an aqueous solution of $Ni(NO_3)_2$ was added to 2 g of the CeO_2–ZrO_2 solid solution, and the mixture was kept on a 353 K steam bath until it dried. Then, it was calcined at 673 K for 30 min. The NiO loadings will be expressed in parentheses: for example, NiO(12.4)/CeO_2–ZrO_2 means 12.4 wt% NiO supported on CeO_2–ZrO_2.

2.2. Partial Oxidation of Methane

A fixed-bed flow reactor made of quartz tubing of 6-mm inner diameter was used. The catalyst was tabletted, pulverized into 10–24 mesh, set in the reactor, and then *in situ* pretreated in a 10%H_2/N_2 stream at 673 K for 30 min. After the catalyst was cooled, a gas mixture composed of 10%CH_4, 5%O_2, and 85%N_2 was allowed to flow at SV 120,000 L/(kg h) and the catalytic performance was measured with gradually increasing reaction temperature from room temperature to 1073 K. Products were analyzed by an on-line Chrompack CP2002 micro gas chromatograph.

2.3. Characterizations

X-ray diffraction (XRD) profiles were recorded on a Shimadzu XD-D1 diffractometer by using Cu $K\alpha$ radiation and a carbon monochrometer. Crystallite sizes of CeO_2, NiO, and ZrO_2 were calculated by the Scherrer equation from half-height width of 111, 012, and 111 diffraction peaks, respectively.

Temperature-programmed reduction was performed in a quartz tube reactor, and hydrogen consumption was measured by a TCD detector: a weighed amount (25 mg) of the sample was placed in the reactor and treated in a 22%O_2–78%He gas mixture at 573 K for 30 min; then, 25 ml/min of the 5% H_2–95%Ar gas mixture was allowed to flow through the reactor. The temperature was increased to 1073 K at a heating rate of 10 K/min. To calibrate the amount of H_2 consumption, the CuO powder supplied by Merck was used.

For some samples, the reduction behavior after re-oxidation was examined. After the first TPR, the sample was cooled down to room temperature, and a 22%O_2–78%He gas mixture was allowed to flow through the reactor for 8 h. Then, the second-cycle TPR measurement was performed. After the second TPR, the sample was cooled down to room temperature and re-oxidized in the 22%O_2–78%He gas flow at 573 K for 30 min (from room temperature to 573 K, 5 K/min). The third-cycle measurement was carried out after the sample was cooled down to room temperature. The fourth-cycle TPR measurement was performed after re-oxidation of the sample in a 22%O_2–78%He gas flow at room temperature for 8 h.

X-ray photoelectron spectroscopy (XPS) was carried out on a Perkin–Elmer Ulvac Phi Model 5500 spectrometer with Mg $K\alpha$ radiation. For the XPS measurement of the reduced catalysts, the sample was heated in an H_2 flow from room temperature to 673 K at a constant heating rate over a period of 2 h and kept in the same gas flow at that temperature for 30 min. Note that the catalyst was handled in open air prior to the XPS measurement. The BET surface area was calculated on the basis of N_2 uptake determined at the liquid nitrogen temperature on a Micrometrics FlowSorb II 2300 analyzer. For the used catalyst, the coke produced during the reaction was removed by combustion at 927 K in air, prior to the N_2 uptake measurement. Thermal analysis was performed on a Shimadzu DTG-50 thermal analyzer, and the temperature was increased to 1073 K at a heating rate of 10 K/min in an air stream of 40 ml/min. The amount of coke formed was calculated from the weight decrease between 423 and 1073 K. FTIR spectra of CO adsorbed on metallic Ni were recorded on a Nicolet Magna IR 560 spectrometer equipped with a diffuse reflectance unit. Samples were reduced *in situ* at 773 K for 30 min in an H_2 stream of 40 ml/min, cooled to room temperature, and then exposed to a 40 ml/min CO flow for 30 min, followed by purging of excess CO by a 40 ml/min He flow for 30 min. The morphology of the coke formed by the reaction was observed on a Hitachi H-800 transmission electron microscope operated at 200 kV.

3. RESULTS AND DISCUSSION

3.1. Redox Property of NiO-Modified CeO_2–ZrO_2 Solid Solutions

The TPR profiles of the catalysts are shown in Fig. 1. A bulk NiO sample supplied by Nacalai Tesque showed reduction peaks at around 693 and 773 K and was quantitatively reduced to metallic Ni below 873 K (Fig. 1(2)). On the other hand, NiO(12.4)/ZrO_2(R) was reduced at 648 and 743 K (Fig. 1(3)), lower than the reduction temperatures for bulk NiO. The amount of H_2 consumption of NiO(12.4)/ZrO_2(R) was 1.88 mmol/g of support, which was in good agreement with the amount of NiO in NiO(12.4)/ZrO_2(R) (1.89 mmol/g of support), indicating that the NiO particles in NiO(12.4)/ZrO_2(R) were also quantitatively reduced to metallic Ni without reduction of ZrO_2(R).

The TPR profile for NiO(12.4)/$Ce_{0.07}Zr_{0.93}O_2$(GT) was quite different from that for NiO(12.4)/ZrO_2(R). A new reduction peak was observed at around 523 K. To investigate

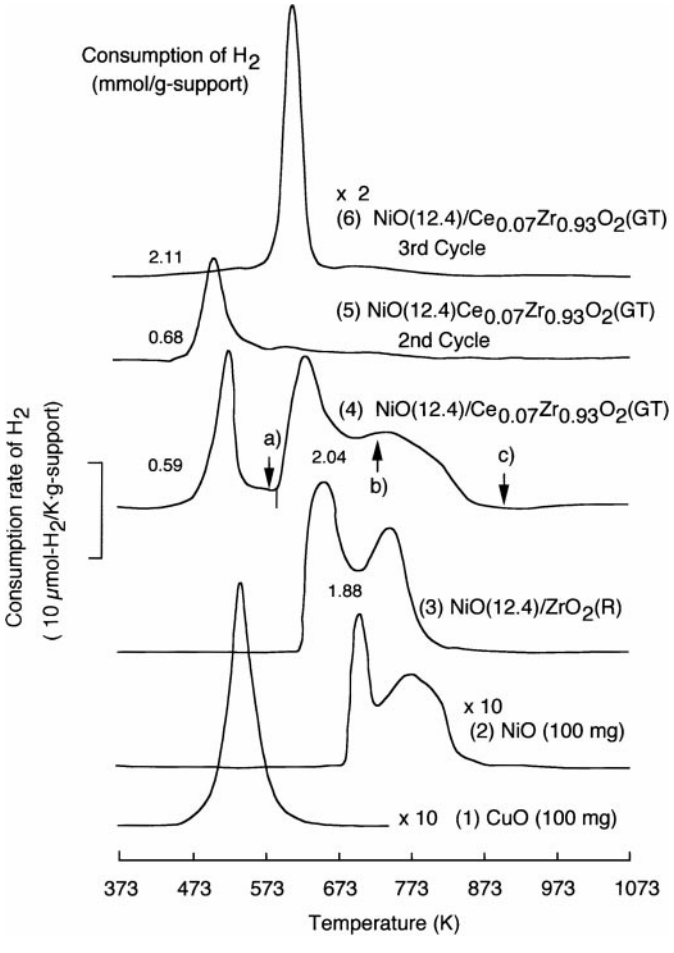

FIG. 1. TPR profiles of NiO/CeO_2–ZrO_2 and NiO/ZrO_2. Conditions: sample, 25 mg; feed, 5%H_2–95%Ar; flow rate, 25 ml/min; heating rate, 10 K/min.

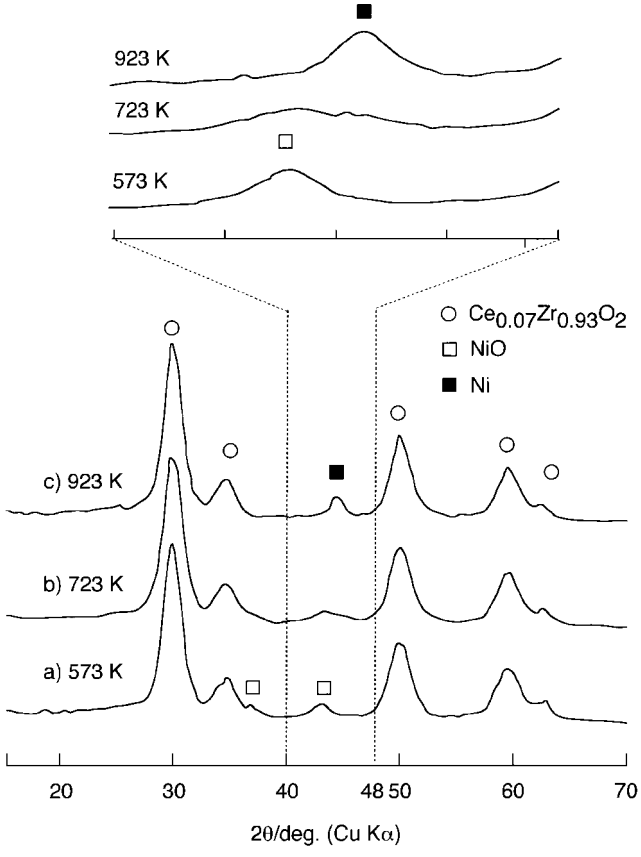

FIG. 2. XRD profiles of NiO(12.4)/$Ce_{0.07}Zr_{0.97}O_2$(GT) quenched at various temperatures during the TPR experiment.

the oxidation state of Ni species, the XRD patterns of the samples quenched at 573, 723, and 923 K (indicated by arrows in Fig. 1) were measured, and the results are shown in Fig. 2. The peak attributed to the metallic Ni was observed at 2θ 44.5° for the sample quenched at 923 K (Fig. 2c), indicating that NiO was completely reduced to metallic Ni below 923 K. Although the sample was handled in open air, NiO was not detected by the XRD measurement. On the other hand, the peak assigned to NiO was observed at 2θ 42.2° for the sample quenched at 573 K, while the sample quenched at 723 K showed both peaks due to NiO and metallic Ni. These results suggested that NiO was reduced to metallic Ni in the temperature range from 573 to 923 K. Therefore, the TPR peak at around 523 K can be attributed to reduction of the support. Since the reduction temperature was low, the peak can be assigned to the surface reduction of the solid solution (9). On the basis of H_2 consumption (0.59 mmol/g of support), chemical composition of the support at 573 K (just before the start of the reduction of NiO) was calculated to be $Ce_{0.07}Zr_{0.93}O_{1.93}$. Moreover, H_2 consumption from 573 to 923 K (2.04 mmol/g of support) was larger than that required for the reduction of NiO to metallic Ni (1.89 mmol/g), indicating that bulk

reduction of $Ce_{0.07}Zr_{0.93}O_{1.93}$ occurred in this temperature range. The final composition of the support was estimated to be $Ce_{0.07}Zr_{0.93}O_{1.91}$ from the total H_2 consumption (0.74 mmol/g of support).

The second-cycle TPR measurement for this sample was performed after the treatment in O_2/He at room temperature; the result is shown in Fig. 1(5). A large peak was observed at 503 K together with a broad signal from 573 to 923 K, but peaks due to the reduction of NiO disappeared. The total H_2 consumption in the second cycle (0.68 mmol/g of support) was a little bit larger than that required for the reduction of the support to $Ce_{0.07}Zr_{0.93}O_{1.91}$ (0.74 mmol/g of support). These results suggest that the reduced solid solution was easily re-oxidized, but only a small amount of metallic Ni was re-oxidized at room temperature. The third-cycle TPR measurement was carried out after treatment in O_2/He at 573 K; the result is shown in Fig. 1(6). Large H_2 consumption suggests that not only reduced support but also a significant amount of Ni was re-oxidized by the O_2/He treatment at 573 K. However, reduction behavior was quite different from that observed at the first TPR measurement (Fig. 1(4)), indicating that the reduction–oxidation cycle completely altered the structure of the NiO(12.4)/$Ce_{0.07}Zr_{0.93}O_2$(GT) catalyst, and this point will be discussed later.

Figure 3 shows the TPR profiles of $Ce_{0.25}Zr_{0.74}O_2$(GT) and $Ce_{0.25}Zr_{0.74}O_2$(CP) without NiO loading. The reduction peaks of $Ce_{0.25}Zr_{0.75}O_2$(GT) were broad and observed at 693 and 823 K (Fig. 3 (1)). These peaks could be assigned to the surface reduction since the peak temperatures were

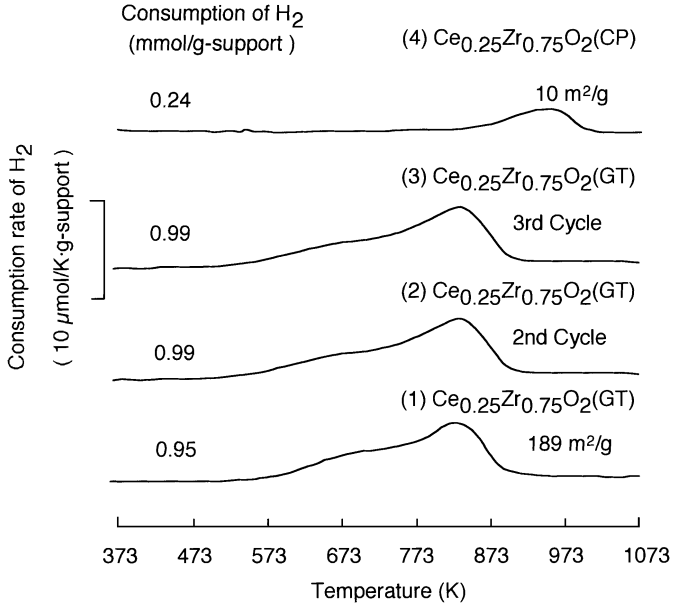

FIG. 3. TPR profiles of large surface area $Ce_{0.25}Zr_{0.75}O_2$(GT) and small surface area $Ce_{0.25}Zr_{0.75}O_2$(CP). Conditions: sample, 25 mg; feed, 5% H_2–95% Ar; flow rate, 25 ml/min; heating rate, 10 K/min.

low. It was shown that bulk reduction of the CeO_2–ZrO_2 solid solution took place above 1073 K (9).

To investigate the nature of the CeO_2–ZrO_2 solid solution, the redox cycles were repeated. The second-cycle TPR profile (i.e., reduction behavior of the sample re-oxidized at room temperature; Fig. 3(2)) was almost identical to the first-cycle TPR profile, indicating that the reduced solid solution was easily re-oxidized at room temperature. This result shows a sharp contrast against the results reported by Fornasiero *et al.* who examined the O_2 uptake on a reduced CeO_2–ZrO_2 solid solution by the pulse method and reported that about 600 K was required to re-oxidize the solid solution (9). The facile re-oxidation of the reduced $Ce_{0.25}Zr_{0.74}O_2$(GT) sample should be caused by its large surface area. The reduction behavior was not altered, even after re-oxidation at 573 K (Fig. 3(3)), indicating that the structure of $Ce_{0.25}Zr_{0.75}O_2$(GT) did not change by oxidation at 573 K.

The TPR peak of $Ce_{0.25}Zr_{0.75}O_2$(CP) (Fig. 3(4)) showed a peak at around 953 K, much higher than that observed for $Ce_{0.25}Zr_{0.75}O_2$(GT), indicating that the former sample was not efficiently reduced. Moreover, the H_2 consumption of the former sample was much smaller than that of the latter, and the former sample was reduced to $Ce_{0.25}Zr_{0.75}O_{1.96}$. This result is in accordance with the argument that hydrogen consumption up to 1073 K is due to surface reduction of the solid solution because the BET surface area of $Ce_{0.25}Zr_{0.75}O_2$(CP) (10 m^2/g) was much smaller than that of $Ce_{0.25}Zr_{0.75}O_2$(GT) (189 m^2/g).

Figure 4 shows the effect of the NiO loadings on the reduction behavior of NiO/$Ce_{0.25}Zr_{0.75}O_2$(GT). When it was modified with a small amount of NiO (0.6 wt%), the reduction peaks shifted to the lower temperature side (543 and 653 K). An increase in the NiO loading caused a further shift of the reduction peaks to 453 and 593 K, indicating that the NiO species promotes the reduction of $Ce_{0.25}Zr_{0.75}O_2$(GT). Similar low-temperature shifts of reduction of support materials by the presence of Ni and platinum-group metals are frequently observed, and this behavior is generally explained by the hydrogen spillover effect (20, 22).

To ensure that the reduction of NiO took place at higher temperatures, the area of the high-temperature peaks of the TPR spectrum, shown by the shadow in Fig. 4, was plotted against the Ni content in NiO/$Ce_{0.25}Zr_{0.75}O_2$(GT). As shown in Fig. 5, the slope of the plot was 1.00, indicating that the shadowed peak(s) quantitatively correlate(s) to the reduction of NiO. On the other hand, the areas of the low-temperature peaks of the TPR spectra, shown without shadow in Fig. 4, were almost identical, suggesting that the surface reduction of the solid solution to $Ce_{0.25}Zr_{0.75}O_{1.88}$ occurred irrespective of NiO loadings. Note that the plot in Fig. 5 had an intercept (0.25 mmol/g of support), indicating that bulk reduction of the solid solution to $Ce_{0.25}Zr_{0.75}O_{1.84}$

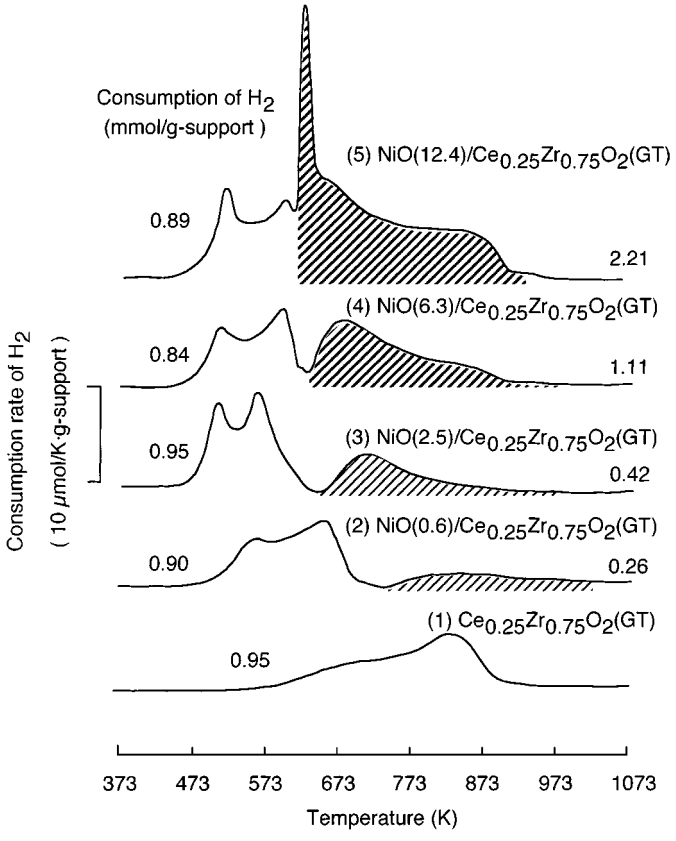

FIG. 4. TPR profiles of NiO/$Ce_{0.25}Zr_{0.75}O_2$(GT) with various Ni loadings. Conditions: sample, 25 mg; feed, 5% H_2–95% Ar; flow rate, 25 ml/min; heating rate, 10 K/min.

took place in the higher temperature range. This may be caused by the hydrogen spillover effect enhanced by the metallic Ni particles formed by reduction of NiO.

Since NiO was not reduced below 573 K, only NiO species were present at the temperature where reduction of $Ce_{0.25}Zr_{0.75}O_2$(GT) started. Therefore, NiO particles apparently facilitated the reduction of the solid solution by the hydrogen spillover effect, although it is generally believed that only metallic Ni has the hydrogen spillover effects (22). In the literature, the spillover effect of NiO was suggested: for example, it was reported that the presence of NiO lowered the reduction temperatures of MoO_3 (23) and WO_3 (24) to 623 and 823–873 K, respectively. As shown in Fig. 1(3), however, reduction of supported NiO started at 623 K; therefore, metallic Ni could be present at the reduction stage of MoO_3 (23) and WO_3 (24). This implies that the possibility for hydrogen spillover from metallic Ni cannot be excluded for these cases. To the best of our knowledge, no report has shown that hydrogen spillover takes place from NiO, and the present paper is the first one that reports that hydrogen spillover occurs from NiO particles as the sole detectable species. There seem to be some possibilities to explain the results. (1) Hydrogen might be dissociatively adsorbed on NiO, and hydrogen atoms were spilled over to CeO_2–ZrO_2 particles. (2) Hydrogen was activated at the point of contact between the NiO and solid solution particles. (3) A small amount of metallic Ni sites, which could not be detected by the TPR experiment, was formed on the surface of NiO particles, and hydrogen spillover took place from the metallic Ni.

The last possibility further requires the explanation why spiltover hydrogen atoms reduced the easily re-oxidized solid solution more easily than the NiO particles present under the metallic Ni sites. Although we cannot differentiate these possibilities at the present stage, it is important to note that the reduction of the $Ce_xZr_{1-x}O_2$ solid solution was facilitated by the presence of NiO particles.

The TPR profiles of NiO(12.4)/$Ce_{0.25}Zr_{0.75}O_2$(GT) after re-oxidation at room temperature are shown in Fig. 6(2). A large peak at 553 K and a small signal around 603 K were observed, but peaks due to the reduction of NiO disappeared. The H_2 consumption was 1.31 mmol/g of support, which was 0.18 mmol/g of support larger than that required for the reduction of the support to $Ce_{0.25}Zr_{0.75}O_{1.84}$ (calculated chemical composition of the support at the end of the first-cycle TPR; 1.13 mmol/g of support). These results again indicate that the reduced solid solution was easily re-oxidized, whereas only a 9.7% portion of metallic Ni was re-oxidized at room temperature. The third-cycle TPR measurement (Fig. 6(3)) indicates that a 79% portion of metallic Ni was re-oxidized at 573 K. However, reduction behavior was quite different from that for the first TPR measurement shown in Fig. 6(1): reduction of NiO and the solid solution at the third cycle took place in the temperature range from 523 to 723 K, and the reduction peak was

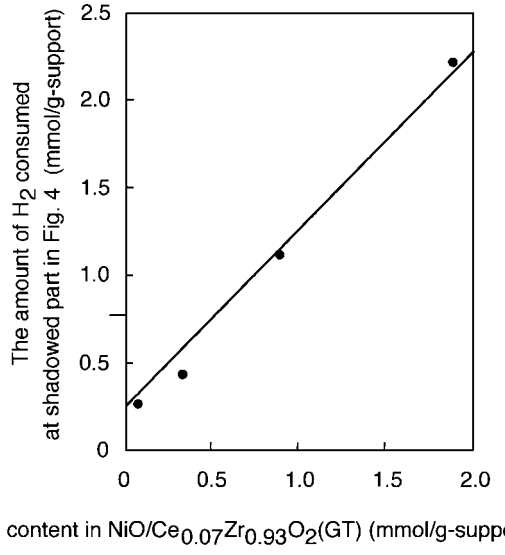

FIG. 5. Relation between the NiO loading and hydrogen consumption in the high-temperature range corresponding to the shadowed peaks in Fig. 4.

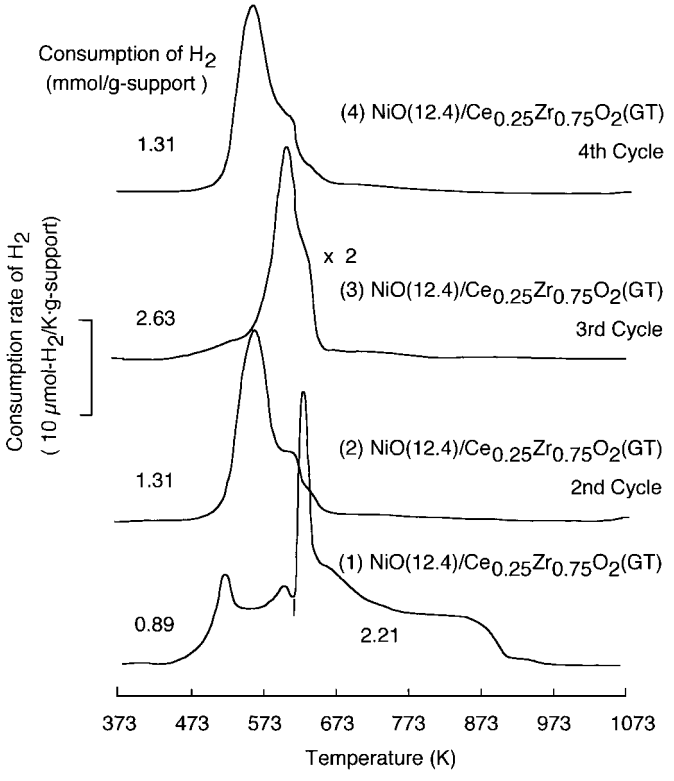

FIG. 6. Recycled TPR profiles of NiO(12.4)/$Ce_{0.25}Zr_{0.75}O_2$(GT). Conditions: sample, 25 mg; feed, 5% H_2–95% Ar; flow rate, 25 ml/min; heating rate, 10 K/min.

sharper than that for the fresh sample. A similar result was also observed in Fig. 1(6) for the solid solution with low Ce contents.

The fourth cycle was performed after the sample was treated in O_2/He at room temperature (Fig. 6(4)). The reduction behavior of $Ce_{0.25}Zr_{0.75}O_2$(GT) in the fourth cycle was almost identical to that for the second-cycle TPR (Fig. 6(2)), indicating that the structure of NiO(12.4)/$Ce_{0.25}Zr_{0.75}O_2$(GT) did not change during the second-cycle and third-cycle TPR measurements. Therefore, the difference observed between (3) and (4) of Fig. 6 can be attributed to the difference in the re-oxidation temperature.

The crystallite size of $Ce_{0.25}Zr_{0.75}O_2$(GT) determined by XRD line broadening slightly increased from 4 to 6 nm during the first-cycle TPR; however, the tetragonal structure of the solid solution did not change. In the first cycle (Fig. 6(1)), the solid solution was reduced in the presence of NiO particles composed of small crystallites (13 nm). On the other hand, the crystallite size of metallic Ni (62 nm) and re-oxidation of the 9.7% portion of metallic Ni before the second cycle (Fig. 6(2)) suggested that a 1-nm film of NiO covered the Ni particle. In the second cycle, solid solution was reduced in the presence of metallic Ni particles. Therefore, reduction of the solid solution took place at lower temperature than that in the first cycle, indicating that metallic Ni particles had a stronger hydrogen spillover effect than NiO particles.

In the third cycle (Fig. 6(3)), the reduction of the solid solution occurred at higher temperature in spite of the fact that metallic Ni particles were present in the sample. On the other hand, the reduction temperature of NiO lowered. These phenomena occurred irrespective of the Ce content in the solid solution. The crystallite size of the solid solution did not change during the second-cycle TPR and re-oxidation treatment at 573 K; however, both large Ni particles and small NiO crystallites were observed for the samples before the third-cycle TPR. The NiO particles with smaller crystallite size were formed from larger metallic Ni particles (62 nm after the second cycle), and a 79% portion of metallic Ni was re-oxidized at 573 K, suggesting that metallic Ni particles were covered with the 12-nm NiO skin layers with the mosaic of the smaller crystallites. Therefore, in the third cycle, the metallic Ni particles cannot interact with gas-phase hydrogen and NiO skin layers had small surface areas, whereas in the first cycle the solid solution was reduced in the presence of smaller crystallite size NiO particles having a large surface area. These arguments can account for the increase in the reduction temperature of the solid solution in the third cycle.

On the other hand, the decrease of the reduction temperature of NiO in the third cycle, as compared with that observed in the first cycle, can be explained by the location of NiO. Whereas the NiO particles were present on the support surface with intimate interaction in first cycle, the NiO crystallites were located on the surface of relatively large metallic Ni particles in the third cycle.

Figure 7 shows the effect of the composition of the CeO_2–ZrO_2 solid solutions upon their reduction behavior. The H_2 consumption below ~573 K, assigned to the surface reduction of the solid solution, increased with an increase in CeO_2 content. Whereas the solid solutions with low CeO_2 contents exhibited only one peak in this region, the solid solutions with high CeO_2 contents showed an additional peak at 603 K. When CeO_2 content is low, most of the next nearest neighbor (NNN) sites from Ce ions should be occupied by Zr ions; therefore, the former peak can be assigned to the reduction of such Ce ions. On the other hand, when CeO_2 content was high, some of the NNN sites of a Ce ion must be occupied by Ce ions; therefore, the peak at 603 K is assigned to the reduction of these Ce species.

The CeO_2 content in the solid solution considerably affected the reduction of NiO. The reduction peaks of the NiO particles supported on ZrO_2 (GT) and $Ce_{0.25}Zr_{0.75}O_2$ (GT) were higher than that of $Ce_{0.07}Zr_{0.93}O_2$ (GT), indicating that the NiO particles supported on ZrO_2 (GT) and $Ce_{0.25}Zr_{0.75}O_2$ (GT) were reduced at higher rates.

By subtraction of the amount of hydrogen required for the reduction of NiO from the total hydrogen consumption,

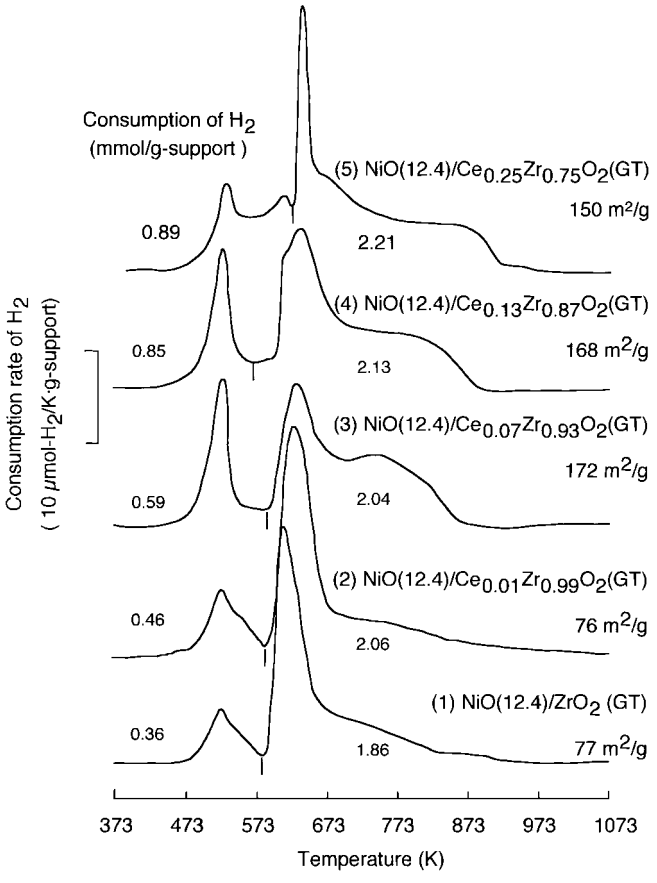

FIG. 7. TPR profiles of NiO catalysts supported on the CeO_2–ZrO_2 solid solutions with various CeO_2 compositions. Conditions: sample, 25 mg; feed, 5% H_2–95% Ar; flow rate, 25 ml/min; heating rate, 10 K/min.

the oxygen storage capacity was calculated, and the results are shown in Fig. 8. The oxygen storage capacity increased with an increase in the Ce proportion in the solid solution, and these values were higher than those reported by Fornaasiero *et al.* (9), when compared at the same Ce proportion. While ZrO_2(R) did not have the oxygen storage capacity (Fig. 1(3)), the oxygen storage capacity of the ZrO_2(GT) was calculated to be 0.04 mol of O/mol of ZrO_2. This value, albeit small, was as large as that reported for ZrO_2 dispersed on the SiO_2 surface (25).

3.2. The Oxidation States of Ni Catalysts Supported on the CeO_2–ZrO_2 Solid Solutions and Their Catalytic Activities for Partial Oxidation of Methane

The activities for methane partial oxidation of the NiO catalysts supported on the CeO_2–ZrO_2 solid solutions were compared, and the results are shown in Table 1. Yields and conversion were based on the following partial oxidation reaction:

$$2CH_4 + O_2 \rightarrow 2CO + 4H_2.$$

Therefore, yields and conversion were defined as follows:

$$CH_4 \text{ conv. } (\%) = \text{output } (CO + CO_2)/\text{input } CH_4 \times 100$$

$$CO \text{ yield } (\%) = \text{output } CO/\text{input } CH_4 \times 100$$

$$H_2 \text{ yield } (\%) = \text{output } H_2/2 \cdot \text{input } CH_4 \times 100.$$

Under the present reaction conditions (SV = 120,000 L/(kg h)), deactivation of the catalysts by coke formation could not be ignored at high temperatures (923 K), and the mass balance for the reaction was not complete because of coke formation. Therefore, catalytic performances at 823 K were compared. NiO(12.4)/ZrO_2(GT) showed a higher activity than NiO(12.4)/ZrO_2(R). The CH_4 conversion and yields of CO and H_2 increased with an increase in CeO_2 proportion of NiO(12.4)/Ce_xZr_{1-x} O_2(GT). These results suggest that the catalytic performance for the partial oxidation of methane (Table 1) increased with an increase in oxygen storage capacities of the support (Fig. 8). It is generally accepted that partial oxidation of methane consists of three primary reactions; i.e., methane combustion reaction and two kinds of reforming reactions of CH_4 with the thus-formed CO_2 and H_2O (4). Since methane combustion was considered to occur by means of the redox mechanism (26), combustion can be promoted by the oxygen storage property of the catalyst support, especially under low partial pressure of oxygen adopted in the present work. This argument implies that combustion of methane is the rate-determining step for the present system.

To evaluate the stability of the crystal structure of the catalyst, the XRD profiles were obtained for the catalysts after use in the partial oxidation reaction run. Fresh ZrO_2(R) had a monoclinic structure, while ZrO_2(GT) and $Ce_xZr_{1-x}O_2$(GT) possessed the tetragonal or cubic structure, and the crystal structures of the catalyst supports were not affected by the reaction. Crystallite sizes of NiO and

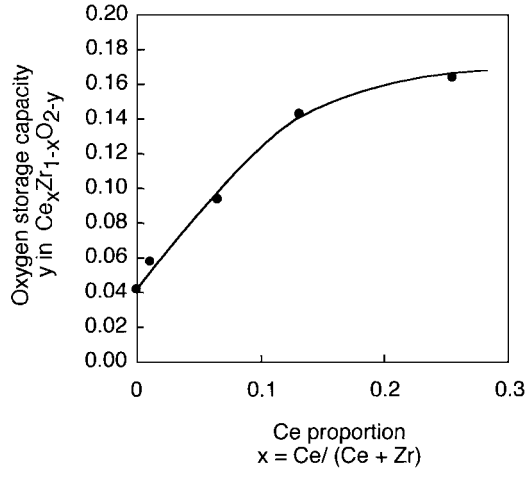

FIG. 8. Relation between Ce proportion in NiO(12.4)/$Ce_xZr_{1-x}O_2$ (GT) and oxygen storage capacity.

TABLE 1

Results of Partial Oxidation of Methane on ZrO_2–CeO_2-Supported Ni Catalysts at High Space Velocity

Catalyst	Temp. (K)	CH_4 conv. (%)	CO yield (%)	H_2 yield (%)	Rate of H_2 production[a] (μmol s^{-1} m^{-2})
NiO(12.4)/ZrO_2(R)	823	9.9	0.8	0.8	0.20
	923	53.0	37.9	35.4	8.78
NiO(12.4)/ZrO_2(GT)	823	32.4	13.0	17.0	0.66
	923	67.8	51.3	57.3	2.21
NiO(12.4)/$Ce_{0.01}Zr_{0.99}O_2$(GT)	823	49.1	28.0	34.6	1.35
	923	59.0	44.1	45.2	1.77
NiO(12.4)/$Ce_{0.03}Zr_{0.97}O_2$(GT)	823	49.7	30.8	39.2	0.89
	923	72.1	59.7	62.8	1.43
NiO(12.4)/$Ce_{0.07}Zr_{0.93}O_2$(GT)	823	50.5	30.1	39.0	0.67
	923	70.8	58.3	59.6	1.03
NiO(12.4)/$Ce_{0.13}Zr_{0.87}O_2$(GT)	823	60.0	38.0	49.9	0.88
	923	75.4	61.1	66.0	1.17
NiO(12.4)/$Ce_{0.25}Zr_{0.75}O_2$(GT)	823	61.6	39.2	51.0	1.01
	923	71.7	56.7	61.6	1.22

Note. Gas composition, 10%CH_4–5%O_2–85%N_2; GHSV, 120,000 l/(kg h). (R) reference sample; (GT) samples prepared by glycothermal method.

[a] Rate was normalized based on surface area before reaction.

ZrO_2 or CeO_2–ZrO_2 are summarized in Table 2. ZrO_2(R) had a large crystallite size (39 nm) and a small BET surface area, which were not altered by their use in the partial oxidation reaction. On the other hand, since ZrO_2(GT) and $Ce_xZr_{1-x}O_2$(GT) had quite large surface areas, they decreased by their use in the partial oxidation of methane; however, relatively large surface areas were preserved after the reaction.

Figure 9 shows the FTIR spectra of CO adsorbed on metallic Ni of the samples prepared by the reduction of NiO/ZrO_2(GT) and NiO/$Ce_xZr_{1-x}O_2$(GT). When the samples were reduced at 673 K, the $Ce_{0.07}Zr_{0.93}O_2$(GT)-supported catalyst showed no peak due to adsorbed CO, while the catalysts supported on the other solid solutions showed a peak at around 2037 cm^{-1} assigned to linear Ni–CO species (27). When the samples were reduced at 773 K, the $Ce_{0.07}Zr_{0.93}O_2$(GT)-supported catalyst exhibited a peak at 2039 cm^{-1}, whereas the other samples showed the peak at the essentially identical wave number that was observed for the catalysts reduced at 673 K. These results indicate that, for the $Ce_{0.07}Zr_{0.93}O_2$(GT)-supported catalyst, back donation from the occupied *d* orbital of metallic Ni to the CO π^* orbital was suppressed (28), which in turn suggests that the electron density of the Ni particles supported on

TABLE 2

Change of the Crystallite Size and BET Surface Areas by Use for Partial Oxidation of Methane

	Crystallite size (nm)[a]					
	NiO		ZrO_2		BET surface area (m^2/g)	
Catalyst	Before reaction	After reaction	Before reaction	After reaction	Before reaction	After reaction[b]
NiO(12.4)/ZrO_2(R)	27	21	39	39	12	14
NiO(12.4)/ZrO_2(GT)	16	20	4	13	77	10
NiO(12.4)/$Ce_{0.01}Zr_{0.99}O_2$(GT)	21	24	4	11	76	7
NiO(12.4)/$Ce_{0.03}Zr_{0.97}O_2$(GT)	19	28	4	9	131	27
NiO(12.4)/$Ce_{0.07}Zr_{0.93}O_2$(GT)	12	17	5	6	172	84
NiO(12.4)/$Ce_{0.13}Zr_{0.87}O_2$(GT)	12	14	4	6	168	80
NiO(12.4)/$Ce_{0.25}Zr_{0.75}O_2$(GT)	13	27	4	6	150	55

Note. (R) reference sample; (GT) samples prepared by glycothermal method.

[a] Crystallite size was calculated by the Scherrer equation.

[b] BET surface area was measured after calcination of the sample at 923 K to remove the produced coke.

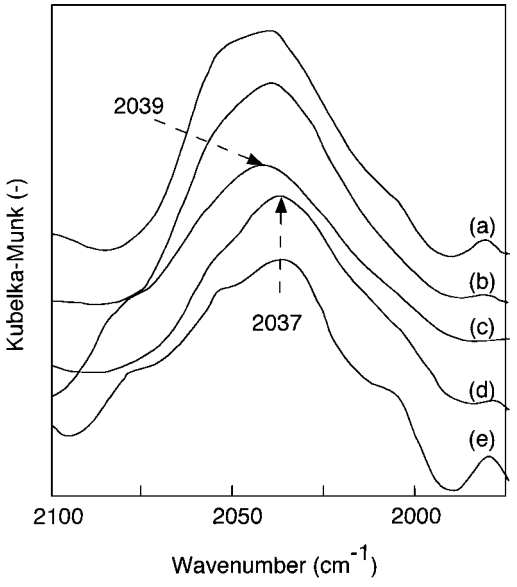

FIG. 9. FTIR spectra of CO adsorbed on Ni particles of the samples prepared by reduction of (a) NiO(12.4)/ZrO_2(GT), (b) NiO(12.4)/$Ce_{0.01}Zr_{0.99}O_2$(GT), (c) NiO(12.4)/$Ce_{0.07}Zr_{0.93}O_2$(GT), (d) NiO(12.4)/$Ce_{0.13}Zr_{0.87}O_2$(GT), and (e) NiO(12.4)/$Ce_{0.25}Zr_{0.75}O_2$(GT) in a H_2 stream at 773 K for 30 min.

lower (i.e., more cationic) than those of the Ni particles supported on the other solid solutions.

To obtain further information about the surface structure of the catalyst, XPS spectra of the catalysts were measured. Binding energies, Ni $2p_{2/3}$, of Ni and NiO species were 852.7 and 853.9 eV, respectively. When both Ni and NiO species were present in the samples, the observed peak could not be separated by deconvolution. Since only NiO species have a shoulder peak at around 856 eV, the proportion of intensity of the 856-eV peak, $I_{856eV}/(I_{856eV} + I_{\sim 852eV})$, was used as a measure of the NiO proportion in the surface region of the Ni species, and the results are summarized in Table 3. For the reduced NiO(12.4)/ZrO_2(GT) sample, a large amount of metallic Ni was present in the surface region of the catalyst. On the other hand, considerable amounts of NiO were detected in the surface of the reduced NiO(12.4)/$Ce_{0.13}Zr_{0.87}O_2$(GT) and NiO(12.4)/$Ce_{0.25}Zr_{0.75}O_2$(GT) samples, suggesting that the surface of Ni particles supported on the solid solutions is easily re-oxidized by treating the catalysts in an ambient atmosphere prior to XPS measurement. Binding energy, Ni $2p_{2/3}$, of the reduced NiO(12.4)/$Ce_{0.07}Zr_{0.93}O_2$(GT) sample,

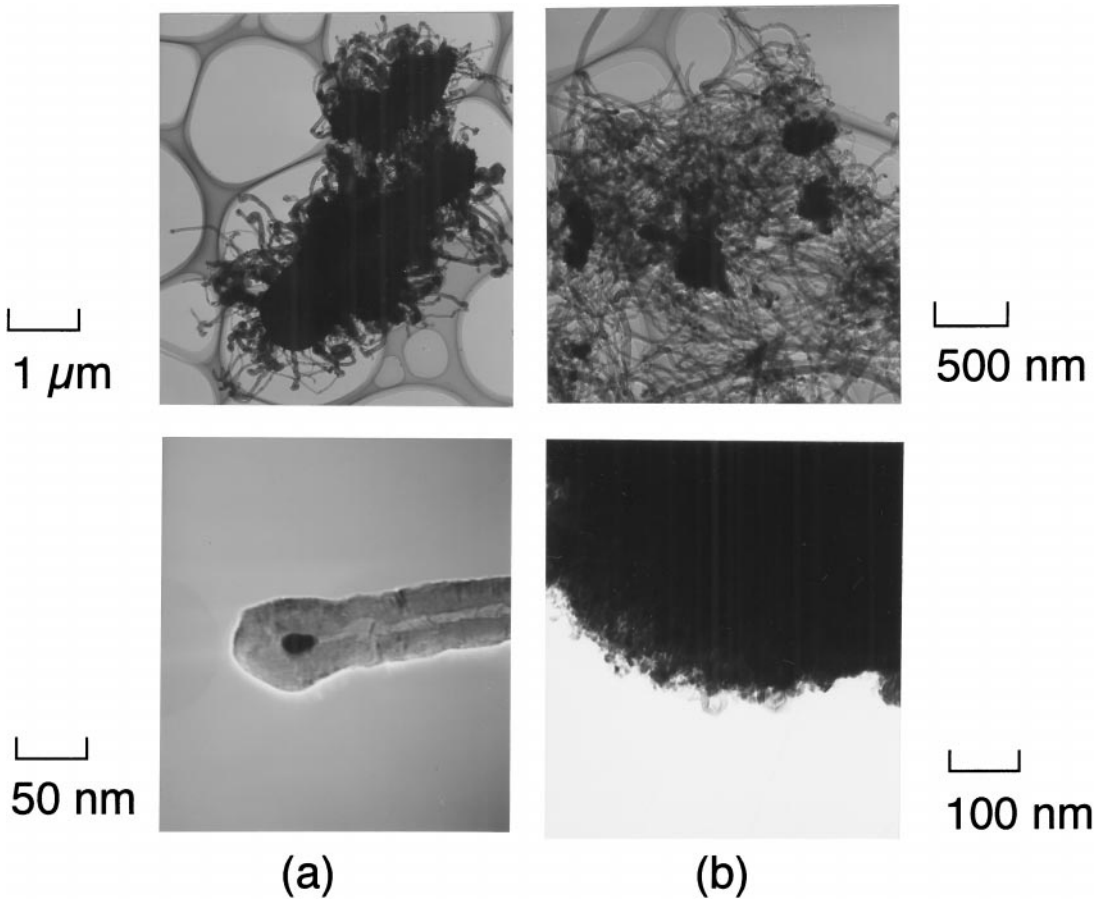

FIG. 10. Transmission electron micrographs of used NiO/CeO_2–ZrO_2. (a) NiO(12.4)/ZrO_2(GT). (b) NiO(12.4)/$Ce_{0.13}Zr_{0.87}O_2$(GT).

TABLE 3

The Amounts of Coke Produced during the Reaction and the Results of XPS Measurement of the Catalyst

Catalyst	Amount of Coke (mg/100 mg of catal.)	Ratio of peak intensity[a] $I_{856eV}/(I_{856eV} + I_{\sim 852eV})$
NiO(12.4)/ZrO_2(GT)	45.32	0.37
NiO(12.4)/$Ce_{0.07}Zr_{0.93}O_2$(GT)	4.53	0.50
NiO(12.4)/$Ce_{0.13}Zr_{0.87}O_2$(GT)	26.51	0.43
NiO(12.4)/$Ce_{0.25}Zr_{0.75}O_2$(GT)	33.59	0.44

Note. (GT) samples prepared by glycothermal method.

[a] Reduction was carried out at 673 K for 30 min; Binding energy of the Ni $2p_{2/3}$ electron of NiO was 853.9 eV with a shoulder peak at 856 eV, while that of Ni was 852.7 eV.

853 eV, and intensity of the 856-eV peak indicate that only NiO species were present in this sample. This result is in good accordance with the results of the FTIR spectrum of adsorbed CO, where the presence of the cationic Ni species was suggested.

The amounts of coke formed by the partial oxidation of methane are also given in Table 3. Of all the catalysts examined, NiO(12.4)/$Ce_{0.07}Zr_{0.93}O_2$(GT) produced the smallest amount of coke during partial oxidation of methane. This result suggests that coke formation is closely connected to the oxidation state of the surface of the Ni species.

Figure 10 shows the TEM images of the coke formed by the reaction. The dark particle in the lower photograph in Fig. 10a was the Ni species encapsulated in the closed end of a nanotube, suggesting that carbon nanotubes are formed by the "tip growth" mechanism (28).

The significant heights of the TPR reduction peaks of NiO supported on ZrO_2(GT) and $Ce_{0.25}Zr_{0.75}O_2$(GT) imply that the NiO particles were reduced rapidly. In contrast, the medium height of the TPR reduction peak of NiO supported on $Ce_{0.07}Zr_{0.93}O_2$(GT) means that the NiO particles were reduced relatively slowly, suggesting that the NiO particles had strong interaction with the support. This result also is in good agreement with the data obtained from FTIR of adsorbed CO and XPS measurement since these two techniques suggested the presence of cationic Ni species. Because of the strong interaction with the support, the Ni particles cannot be "lifted off," and therefore the catalyst produced a relatively small amount of coke.

4. CONCLUSION

Surface reduction of the large surface area CeO_2–ZrO_2 solid solutions prepared by the glycothermal method occurred at 623–773 K, which was much lower than that observed for the solid solution prepared by the conventional method. Reduction and re-oxidation cycles of the large surface area CeO_2–ZrO_2 solid solution did not change the structure, and the reduced solid solution was easily re-oxidized, even at room temperature. The NiO loading lowered the reduction temperature of the solid solution, and reduction started in the presence of NiO species. Apparent hydrogen spillover effect was suggested for NiO particles, although a small amount of reduced NiO sites, which could not be detected, might possibly show hydrogen spillover effect. The catalytic activities of the NiO catalyst supported on the solid solution for the partial oxidation reaction of methane increased with an increase in the oxygen storage capacity of the support, which indicates that this reaction proceeded by means of the redox mechanism. Ni particles having a weak interaction with the support had a metallic feature and produced large amounts of coke (carbon nanotubes). On the other hand, the Ni particles having a strong interaction had a cationic nature and produced a small amount of coke.

ACKNOWLEDGMENT

This work was partly supported by a Grant-in-Aid for Encouragement of Young Scientists from the Ministry of Education, Science, Sports and Culture, Japan (No. 11750674).

REFERENCES

1. Taylor, K. C., *Catal. Rev.-Sci. Eng.* **35**, 457 (1993).
2. Summers, J. C., and Ausen, S. A., *J. Catal.* **58**, 131 (1979).
3. Yao, H. C., and Yu Yao, Y. F., *J. Catal.* **86**, 254 (1984).
4. Dissanayake, D., Rosynek, M. P., Kharas, K. C. C., and Lunsford, J. H., *J. Catal.* **132**, 117 (1991).
5. Tang, S., Lin, J., and Tan, K. L., *Catal. Lett.* **51**, 169 (1998).
6. Diskin, A. M., Cunningham, R. H., and Ormerod, R. M., *Catal. Today* **46**, 147 (1998).
7. Inui, T., Saigo, K., Ichino, K., Takami, T., Takeguchi, T., Iwamoto, S., and Fujii, Y., *Ceram. Trans.* **73**, 39 (1997).
8. Inui, T., Ichino, K., Matsuoka, I., Takeguchi, T., Iwamoto, S., Pu, S., and Nishimoto, S., Korean *J. Chem. Eng.* **14**, 441 (1997).
9. Fornaasiero, P., Di Monte, R., Rao, G. R., Kašpar, J., Meriani, S., Trovarelli, A., and Graziani, M., *J. Catal.* **151**, 168 (1995).
10. Fornaasiero, P., Balducci, G., Di Monte, R., Kašpar, J., Sergo, V., Gubitosa, G., Ferrero, A., and Graziani, M., *J. Catal.* **164**, 173 (1996).
11. Fornaasiero, P., Kašpar, J., Sergo, V., and Graziani, M., *J. Catal.* **182**, 56 (1999).
12. Vlaic, G., Di Monte, R., Fornaasiero, P., Fonda, E., Kašpar, J., and Graziani, M., *J. Catal.* **182**, 378 (1999).
13. Fornaasiero, P., Fonda, E., Di Monte, R, Vlaic, G., Kašpar, J., and Graziani, M., *J. Catal.* **187**, 177 (1999).
14. Fornaasiero, P., Hickey, N., Kašpar, J., Dossi, C., Gava, D., and Graziani, M., *J. Catal.* **189**, 326 (2000).
15. Fornaasiero, P., Hickey, N., Kašpar, J., Montini, T., and Graziani, M., *J. Catal.* **189**, 339 (2000).
16. Hoang, H.-L., Berndt, H., and Lieske, H., *Catal. Lett.* **31**, 165 (1995).
17. Shishido, T., and Hattori, H., *Appl. Catal. A* **146**, 157 (1996).
18. Inoue, M., Sato, K., Nakamura, T., and Inui, T., *Catal. Lett.* **65**, 79 (2000).
19. Inoue, M., Kominami, H., and Inui, T., *Appl. Catal. A* **97**, L25 (1993).
20. Sermon P. Q., and Bond, G. C., *Catal. Rev.* **8**, 211 (1973).

21. Otsuka, K., Ye, W., and Nakamura, M., *Appl. Catal. A* **183**, 317 (1999).
22. Bianchi, D., Gardes, G. E. E., Pajonk, G. M., and Teichner, S. J., *J. Catal.* **38**, 135 (1975).
23. Masson, J., Delmon, B., and Nechtshein, J., *Acad. Sci. Paris* **266**, 428 (1968).
24. Samsonov, G. V., Lambiev, D. K., Pangarova, V. Kh., and Tomova. T. T., *Konf. Met. Proszkow Rev. 3rd* **1**, 325 (1971).
25. Borer, A. L., Brönnimann, C., and Prins, R., *J. Catal.* **145**, 516 (1994).
26. Hicks, R. F., Qi, H., Young, M. L., and Lee, R. G., *J. Catal.* **122**, 295 (1990).
27. Priment, M., Dalmon, J. A., and Martin, G. A., *J. Catal.* **46**, 25 (1977).
28. Dung, N. T., Tichit, D., Chiche, B. H., and Coq, B., *Appl. Catal. A* **169**, 179 (1998).
29. Cassell, A. M., Raymakers, J. A., Kong, J, and Dai, H., *J. Phys. Chem. B* **103**, 6484 (1999).